Published in final edited form as:
Anal Chem. 2013 April 2; 85(7): 3599–3605. doi:10.1021/ac3033849.

Dynamic full-field infrared imaging with multiple synchrotron beams

Eli Stavitski[a,§], **Randy J. Smith**[a], **Megan W. Bourassa**[b], **Alvin S. Acerbo**[c], **G. L. Carr**[a], and **Lisa M. Miller**[a,b,c,*]

[a]Photon Sciences Directorate, Brookhaven National Laboratory, Upton, NY 11973, USA

[b]Department of Chemistry, Stony Brook University, Stony Brook, NY 11794, USA

[c]Department of Biomedical Engineering, Stony Brook University, Stony Brook, NY 11794, USA

Abstract

Microspectroscopic imaging in the infrared (IR) spectral region allows for the examination of spatially resolved chemical composition on the microscale. More than a decade ago, it was demonstrated that diffraction limited spatial resolution can be achieved when an apertured, single pixel IR microscope is coupled to the high brightness of a synchrotron light source. Nowadays, many IR microscopes are equipped with multi-pixel Focal Plane Array (FPA) detectors, which dramatically improve data acquisition times for imaging large areas. Recently, progress been made toward efficiently coupling synchrotron IR beamlines to multi-pixel detectors, but they utilize expensive and highly customized optical schemes. Here we demonstrate the development and application of a simple optical configuration that can be implemented on most existing synchrotron IR beamlines in order to achieve full-field IR imaging with diffraction-limited spatial resolution. Specifically, the synchrotron radiation fan is extracted from the bending magnet and split into four beams that are combined on the sample, allowing it to fill a large section of the FPA. With this optical configuration, we are able to oversample an image by more than a factor of two, even at the shortest wavelengths, making image restoration through deconvolution algorithms possible. High chemical sensitivity, rapid acquisition times, and superior signal-to-noise characteristics of the instrument are demonstrated. The unique characteristics of this setup enabled the real time study of heterogeneous chemical dynamics with diffraction-limited spatial resolution for the first time.

Keywords

synchrotron; infrared microspectroscopy; imaging; FTIR; focal plane array; dynamics

1. Introduction

Vibrational spectroscopy is one of the most powerful techniques for chemical analysis due to its excellent chemical sensitivity. Among vibrational methods, Fourier-Transform Infrared (FTIR) spectroscopy in the mid infrared region has extensive applications across many fields, including chemistry, biology, geology, materials, and environmental science,

*Corresponding Author: Lisa M. Miller, lmiller@bnl.gov, fax: +1 631 344 3238 .
§Current address: Canadian Light Source, 44 Innovation Boulevard, Saskatoon, SK, S7N 2V3, Canada

Supporting Information
Detailed experimental procedures for spinal cord preparation, calculation of the number of infrared source segments, and the calculation of infrared extraction efficiency (i.e. figure-of-merit).

allowing direct compositional and quantitative information to be obtained without introducing unintentional perturbations to the sample. Integration of FTIR with microscopic imaging techniques provides a tool capable of visualizing the spatial distribution of the sample constituents.[1] FTIR microspectroscopy is of considerable interest for biochemical analysis since staining of the samples is not required.[2-3] In comparison with Raman scattering based microscopy, FTIR microspectroscopy can often be more sensitive, eliminating detrimental effects such as fluorescence, which can obscure Raman scattering, and radiation damage due to prolonged exposures to high intensity lasers.

Conventional FTIR microspectroscopy (FTIRM) relies on a combination of a thermal (globar) infrared (IR) source, a rapid-scan interferometer, a microscope featuring all-reflective (Schwarzschild or Cassegrain-type) optics, and a single element photoconductive mercury cadmium telluride (MCT) detector. Spectral images are obtained by raster-scanning the sample through a beam that is confined by an aperture with desired dimensions. The performance of such an instrument is determined by the photon flux of the globar source through the aperture, effectively limiting the spatial resolution to 20-30 μm. Replacing the thermal source with a synchrotron source has dramatically improved the efficiency of FTIRM data collection when the spatial resolution reaches the diffraction limit.[5] The synchrotron light in the mid-IR spectral region of bending magnet radiation provides an overall photon flux comparable to a thermal source. However, the synchrotron's effective source dimension and emission angles are very small, allowing the microscope's apertures to define a diffraction-limited sample area while retaining excellent photon throughput and a high signal-to-noise ratio (SNR).[6]

About 20 years ago, the arrival of a 2-dimensional multi-pixel mid-infrared detector – often referred to as a Focal Plane Array (FPA) – greatly enhanced the capabilities of FTIR spectroscopic imaging.[7] Originally developed for military and surveillance applications, these photovoltaic (photodiode) detector arrays are now available in commercial FTIR microscopes. In the early stages, slow FPA data acquisition and readout speed restricted spectrometer operations exclusively to "step-scan" mode; with new developments, rapid-scan measurements are now routinely performed.[8] With simultaneous data collection from all the detector pixels, acquisition times for large areas of the sample can be reduced dramatically without compromising the spatial resolution and spectral quality. The current state of this multi-pixel approach, which is frequently called FTIR imaging (FTIRI), has recently been reviewed.[4]

The combination of a high-throughput multi-pixel detector with the bright synchrotron light source is appealing. However until recently, little progress in this area has been made. Several groups reported results on the feasibility of coupling an FPA to a synchrotron source,[9-10] but a thorough comparison of the spectral quality or spatial resolution was not included. It has become apparent that, with standard IR beamline optics, only a small area of the FPA can be homogeneously illuminated.[10] Due to the extended source depth of the dipole magnet radiation collected by the beamline front-end optics, only a portion of light within the limited horizontal acceptance range matches the microscope optics. In another approach, defocusing the synchrotron beam illuminates a significantly large FPA region, but the high brightness advantage of the traditional synchrotron IR beamline is lost. As an alternative, Carr et al. proposed a scheme to fill a significant portion of the detector without defocusing by collecting four segments of the source arc that are collimated separately and imaged together at the sample position.[11] This idea was recently optimized and implemented at the IRENI beamline (Synchrotron Radiation Center, Wisconsin), where customized beamline optics were designed to deliver 12 individual source segments to the FPA detector.[12]

While IRENI is an elegant approach that allows for a very large horizontal extraction of dipole synchrotron radiation, the design involves a complex system of optics and windows that share the ultra-high vacuum environment of the synchrotron storage ring. Synchrotrons operating at higher beam currents should be capable of competitive performance using less horizontal extraction, in which case a simpler and less expensive design is feasible. In what follows, we describe how a conventional mid-IR synchrotron beamline, U10 at the at the National Synchrotron Light Source (NSLS) vacuum ultra violet infrared (VUV-IR) ring, was easily modified to allow for the uniform filling of a significant portion of an FPA detector. diffraction-limited imaging is demonstrated, as well as spatial oversampling that is essential for image reconstruction by deconvolution. The optimized SNR and the data acquisition rates attainable with this instrument are used to demonstrate real-time imaging of chemical transformations on a micrometer scale.

2. Experimental

The U10 beamline extracts 85 mrad (horizontal) × 40 mrad (vertical) of radiation from a bending magnet (Figure 1a). The VUV-IR ring (bending radius = 191 cm) meets or exceeds the natural opening angle for frequencies down to 250 cm^{-1} for complete coverage of the mid-IR spectral range (see the Supplemental Information for details). The radiation fan is collected by a water cooled flat mirror followed by an ellipsoidal mirror that delivers the beam through a wedged diamond window to an intermediate focus outside of the synchrotron's ultra-high vacuum environment.

In order to reconfigure the synchrotron source into an optimal format for the FPA, the approach was to optimize the collimation of individual source segments without sacrificing the intrinsic source brightness and then utilize diffraction-blurring at the sample plane to achieve reasonably homogeneous illumination. For beamline U10, the source was divided into four segments as explained further in the Supplemental Information. Source segments were collimated individually using four staggered 63.5 cm focal length spherical mirrors placed in a beam matching optics box, as shown in Figure 1b. The separation between the spherical mirrors (~ 4 cm) was chosen to cover the entire length of the source arc (85 mrad horizontal extraction corresponds to ~18 cm length). Each of the four nearly collimated beams are reflected from individual plane elements of a 2×2 segmented mirror and then transported to a Bruker Vertex 80 spectrometer, interfaced with a Bruker Hyperion 3000 microscope. The combination of spherical and segmented mirrors provides full and independent steering of each beam.

We selected a 15× Spectra-Tech Reflachromat™ with an adjustable back conjugate focal distance for use as a condenser to illuminate the sample. Its numerical aperture (NA) of 0.58 is a close match to that of the 74× Ealing objective (0.65 NA) used to project the image on the FPA. The microscope was equipped with a photovoltaic mercury-cadmium-telluride (MCT) 128×128 Santa Barbara Focal Plane array detector with a 40 μm pixel spacing. With this optical configuration, an area of 36×36 pixels was illuminated, corresponding to 20×20 μm on the sample (Figure 1c-d). It should be noted that illuminating larger areas of the array might not bring an immediate advantage; for the detector readout electronics used in Bruker FPA equipped microscopes, restricting the size of the active area to 32 pixels vertically allows the detector readout rates to be increased two-fold compared to a 64 pixel-tall area. In order to achieve a larger field of view and a lower pixel resolution (1.1 Nm), a lower magnification objective (e.g. 36×) can be used.

Imaging measurements with a globar source were performed with the same Bruker instrument, as well as with a Perkin Elmer Spectrum Spotlight microscope equipped with a 16-element quasi linear, photoconductive MCT detector array. In the latter case, the IR

objective magnification yielded an effective pixel dimension of 6.25×6.25 μm. Two test patterns were used to benchmark the optical performance and spatial resolution of the instrument, i.e., Ealing's "Silver Points" pattern consisting of 0.5-5 μm pinholes in Cr thin film on glass, and Edmund Optics United States Air Force (USAF) resolution test pattern with 228 line pairs per mm as the smallest line features. For each frame, 32 scans were collected. Cryosectioned mouse spinal cord tissue samples were also used to demonstrate the diffraction-limited spatial resolution. Mouse experiments were approved by the University of Florida Institutional Animal Care and Use Committee and specimens were prepared via a standard procedure described in the Supplemental Information.

The excellent SNR made available with the high-brightness synchrotron source allowed for short scan times and thus the opportunity for imaging chemical processes in real-time. To demonstrate this, we investigated the real-time photo-oxidation of small polystyrene beads. Polymer spheres (Polysciences, Inc. Fluoresbrite® Yellow Green Microspheres, 5 μm diameter) were dispersed on a CaF_2 slide and illuminated using unfiltered light from X-Cite Fluorescence Light Source (Lumen Dynamics) for a period of 14 hours and images were collected every 30 min (128 scans/90 sec per frame, 8 cm^{-1} resolution).

3. Results and Discussion

FTIR spectroscopic imaging with a synchrotron source is typically performed in the raster-scan mode with an aperture that constrains the illuminated region. Due to the flux limitations and the desired spectral range, including the fingerprint region, measurements are seldom performed with apertures smaller than 3-4 μm. With a confocal arrangement, i.e. confining both illumination and collection light paths, one can achieve a spatial resolution of $\lambda/2$.[13] It is therefore difficult to achieve truly diffraction-limited performance for the shortest wavelengths in the mid-IR region (4000 cm^{-1} or 2.5 μm). With a 74× objective, each FPA detector pixel samples a 0.54×0.54 μm area on the sample plane, allowing for at least double oversampling of the diffraction-limited images across the mid-IR spectral range. Oversampled images are amenable for computational recovery/enhancement of spatial resolution using deconvolution methods; this mathematical reconstruction has found wide usage in, for example, fluorescence and X-ray microscopy.[14-15]

In order for the deconvolution procedure to yield an accurate result, the determination of the optical system's point spread function (PSF) is essential. This PSF describes how the ultimate signal intensity at the sample location is distributed in the image plane. We have evaluated the PSF of the microscope objective by imaging a 2 μm pinhole (Cr/glass) (Figure 2a). The images shown in Figure 2b-c represent the integrated transmission intensities over 3200-3000 and 2350-2150 cm^{-1}, respectively. Longer wavelengths were not accessible due to the absorption cutoff of the glass substrate. These images can be compared to the theoretically predicted images (Figure 2d-e), which show the convolution of a computer-generated pinhole image and the PSF of the 74× objective calculated with ZEMAX™ optical design software for 3100 and 2250 cm^{-1}. The pattern exhibiting significant intensity outside the zero-order peak is due to the central obscuration of the Schwarzschild-type optics. The nearly homogeneous intensity in the first-order ring (Figure 2b) indicates that the synchrotron beams uniformly fill the condenser optics. The three-fold pattern in the Figure 2c is due to the "spider" mount of the small mirror of the Schwarzschild objective.

To determine the optical performance of the FPA-based instrument, FTIR images of the 1951 USAF test target were taken in a transmission geometry. Integrated intensities over 3200-3000 and 2350-2150 cm^{-1} are shown in Figure 2f and 2h. Notice that the smallest features (2.2 μm lines spaced at 2.2 μm) are resolved even at the longer wavelengths (dashed line in Figure 2h, bottom right corner). For the case of aperture-based FTIRM, the

spatial resolution is estimated as 2λ/3 and λ/2 for single- and confocal aperture systems, respectively (approx. 3.0 to 2.2 μm at 2200 cm^{-1}).[13] Therefore, the instrument's optical performance matches that of a confocal IR microscope.

With the PSF of the system evaluated, we performed image restoration using a spatial deconvolution algorithm. Figures 2g and 2i show the results of the Lucy-Richardson-based PSF deconvolution[16-17] using the theoretical PSF. This iterative procedure, based on the maximum-likelihood approach, accounts for Poisson-distributed noise, which appropriately describes noise resulting from photon counting on the detector. One can see that, in the deconvolved image integrated between 2350 and 2150 cm^{-1} (see inset in Figure 2i), the 2.2 μm spaced features are completely resolved, indicating that sub-diffraction spatial resolution was attained. It should be emphasized that other deconvolution methods, e.g. those based on Fourier Filtering, can be applied depending on the PSF precision and the noise levels.[18]

To demonstrate the chemical imaging capabilities of the instrument with the globar vs. synchrotron IR source, we scanned a mouse spinal cord cross section using FTIRI (Figure 3). The major components of the spinal cord tissue, e.g. gray and white matter, can be chemically differentiated based on their IR spectral signatures. Absorption in the C-H stretching region is significantly higher in the lipid-rich white matter, which is attributed to the CH_2 and CH_3 stretching vibrations predominantly arising from the lipid alkyl chains. In grey matter, the lipid content is lower and the protein-rich neuronal cell bodies predominate the spectra.[19] Therefore, by taking a ratio of the integrated spectral intensities from the lipids (C-H stretch regions) and protein (i.e. Amide I band), the two spinal cord regions can be readily visualized. Anatomically, the gray matter extends into the white matter by means of small tracts that are responsible for relaying signals to and from the brain. These tracts are comprised of narrow neuronal axons, and the ability to study their structure and composition can be greatly enhanced with sub-diffraction IR imaging. This is particularly important since these axonal tracts are degraded in neurodegenerative diseases, such as Alzheimer's disease and amyotrophic lateral sclerosis.[20]

Figures 3a-d compare the visible microscope image of the stained spinal cord cross-section, the FTIRI data acquired with the globar linear array microscope, and the synchrotron FPA system. The ratio of the integrated absorption intensities for lipids (C-H stretch, 3000-2800 cm^{-1}) and protein (Amide I band, 1710-1600 cm^{-1}) are shown, demonstrating the spatial variation that can only be detected with smaller FPA pixels. The gray matter tracts are typically 10-15 μm in width, which corresponds to 2-3 pixels in the linear array; therefore, the correct dimensions of the tract, the extent of its penetration into the white matter, and its composition are not well distinguished with the linear array. In addition, the images are displayed with the same intensity color scale, where the deeper blues and reds emphasize the superior contrast of the synchrotron FPA system (Figure 3d). Enhanced chemical contrast can also be observed in the spectra recorded across the track (Figures 3e-f). With the globar source, very little variation in the spectra can be observed due to cross contamination of the spectra from adjacent regions. In contrast, the spectral differences in the lipid/protein peak ratios can easily be elucidated in the synchrotron FPA data.

The improved SNR attainable with the synchrotron FPA configuration also leads to enhanced sensitivity, as illustrated in Figure 3g, where spectra from a single pixel are compared between the FPA with both the globar and synchrotron sources and the linear array with the globar source. For comparison purposes, we estimated the apparent SNR for the spectra as a ratio of the Amide I peak absorption maximum at ~1655 cm^{-1} to the peak to peak noise values in the baseline (2000-1900 cm^{-1}). First, one can see an 11-fold improvement when the synchrotron replaces the thermal source in the FPA instrument (Figure 3g (i) vs. (iii)). When larger pixels are sampled, the value is anticipated to

improve.[21] Therefore, the comparison of the globar source with the FPA vs. linear array detector (0.54 μm vs. 6.25 μm vs. pixel size) yields approximately a 6-fold improvement in the apparent SNR (Figure 3g (i) vs. (iv)). To the best of our knowledge, this is the first time a direct comparison between the two IR sources with the same instrument has been made.

One of the most attractive possibilities arising from the synchrotron FPA IR detector is the full-frame time-lapsed chemical imaging of dynamic processes. Although the feasibility of probing transient processes with single-pixel IR microspectroscopic measurements has been demonstrated, continuous raster-scanning of large areas limits the temporal resolution due to long acquisition times.[22] Therefore, the temporal evolution of a spectrum at a single spot on the sample is usually reported.[23-25] To demonstrate the feasibility of this imaging mode, we followed the photodegradation of 5 μm polystyrene (PS) beads under UV irradiation (Figure 4a), tracking the chemical changes related to the polymer chain decomposition over time. Photodegradation is the main process of polymer weathering and accounts for the majority of product failures; therefore, mechanistic studies are necessary for plastic lifetime prediction and stabilizer optimization.[26] Several photo-oxidation pathways have been proposed for polystyrene, and there are a number of spectral features that can be detected with FTIR spectroscopy. Here, photoinduced cleavage and oxidation of the polymer backbone resulted in a decrease in the C-H absorption peaks as well as the appearance of a broad band between 1650-1850 cm^{-1} due to a mixture of oxygenated products, including monomeric and chain carboxylic acids and esters. Figures 4b and 4c show the FTIR images of a cluster of PS beads at different irradiation times. Specifically, Figure 4b shows the disappearance of the C-H stretch (3050-3000 cm^{-1}) and Figure 4c shows the appearance of the broad carbonyl band (1620-1815 cm^{-1}) over the course of 14 hours. The spectra averaged over a 3×3 pixel area (2.6 μm^2) from one PS bead are shown in Figures 4d-e, confirming the decrease in the aromatic and aliphatic C-H stretching bands and the appearance of the oxygen containing products. The induction period, lasting for the first 100-150 min of the reaction, can be observed in the kinetic curves in Figure 4f, and the steady state in the carbonyl concentration was reached after ca. 8 hours of irradiation, which is consistent with previous findings.[27-28] While the spectral data shown is a convolution of the absorption features and scattering effects from the spherical beads,[4] we integrated over narrow spectral ranges to plot the images in Figures 4b and 4c and to calculate the kinetic traces. It should be emphasized that, even though this photo-oxidation process occurred over many hours, each full FPA frame was recorded in less than two minutes with a high SNR, indicating that much faster chemical or biological transformations could also be probed. In addition, while in the present case no spatial differences among the beads were observed, the method has the potential to show heterogeneity in ensembles of particles or living cells on a scale of a few microns.

4. Conclusions and Outlook

By optical matching of the synchrotron source to the FPA FTIR microscope using a simple 4-beam configuration for “slicing” the bending magnet radiation, we have achieved diffraction-limited imaging across the mid-IR spectral region with exceptional SNR. While the exact optical configuration is determined by factors including bending magnet radius, horizontal and vertical extraction angles, and extraction optics, we have shown that our approach can be implemented on most existing IR synchrotron beamlines without elaborate or expensive optical schemes.

With this instrument configuration, image oversampling can be used with image restoration algorithms for recovering spatial information lost due to diffraction. Chemical transformations can be monitored in time and space with frame rates that are beyond the capabilities of the single element detector instruments. In the future, widespread adoption of

time-lapsed synchrotron/FPA IR imaging will require the development of environmental chambers that are compatible with the stringent requirements of the sample and IR microscope optics. In particular, high-magnification Schwarzschild objectives have short working distances that are typically less than a few millimeters, and high numerical apertures that necessitate wide opening angles. Ongoing developments of versatile chambers for *in vivo* IR imaging of biological specimens will push the boundaries of this rapidly developing technique.[22, 24, 29-30] Beyond the biomedical field, studies of chemical transformations, e.g. catalytic reactions,[23, 31] in a spatially resolved manner will benefit from full-field FTIR imaging provided that an *in-situ* reaction cell that allows for accurate control of reaction conditions is designed. With these future developments, dynamic synchrotron FTIR imaging will become an important tool in a variety of disciplines.

Supplementary Material

Refer to Web version on PubMed Central for supplementary material.

Acknowledgments

This research, performed at the National Synchrotron Light Source beamline U10, was supported by the National Institutes of Health grant RR23782. The NSLS is supported by the US Department of Energy under Contract No. DE-AC02-98CH10886.

References

1. Levin IW, Bhargava R. Annual Review of Physical Chemistry. 2005; 56:429–474.
2. Fernandez DC, Bhargava R, Hewitt SM, Levin IW. Nature Biotechnology. 2005; 23:469–474.
3. Miller LM, Dumas P. Biochimica et Biophysica Acta. 2006; 1758:846–857. [PubMed: 16781664]
4. Bhargava R. Applied Spectroscopy. 2012; 66:1091–1120. [PubMed: 23031693]
5. Carr GL. Vibrational Spectroscopy. 1999; 19:53.
6. Duncan WD, Williams GP. Applied Optics. 1983; 22:2914–2923. [PubMed: 18200130]
7. Lewis EN, Treado PJ, Reeder RC, Story GM, Dowrey AE, Marcott C, Levin IW. Analytical Chemistry. 1995; 67:3377–3381. [PubMed: 8686889]
8. Huffman SW, Bhargava R, Levin IW. Applied Spectroscopy. 2002; 56:965–969.
9. Moss D, Gasharova B, Mathis Y-L. Infrared Physics and Technology. 2006; 49:53–56.
10. Petibois C, Cestelli Guidi M, Piccinini M, Moenner M, Marcelli A. Analytical and Bioanalytical Chemistry. 2010; 397:2123–2129. [PubMed: 20517599]
11. Carr, GL.; Miller, LM.; Dumas, P. Biomedical Applications of Synchrotron Infrared Microspectroscopy. Moss, D., editor. RSC Publishing; Cambridge; 2011. p. 225
12. Nasse MJ, Walsh MJ, Mattson EC, Reininger R, Kajdacsy Balla A, Macias V, Bhargava R, Hirschmugl CJ. Nature Methods. 2011; 8:413–U58. [PubMed: 21423192]
13. Carr GL. Review of Scientific Instruments. 2001; 72:1613–1619.
14. Lacoste TD, Michalet X, Pinaud F, Chemla DS, Alivisatos AP, Weiss S. Proceedings of the National Academy of Sciences. 2000; 97:9461–9466.
15. Swedlow, JR. Digital Microscopy. 3rd Edition. Sluder, G.; Wolf, DE., editors. Vol. 81. Elsevier Academic Press Inc; San Diego: 2007. p. 447+
16. Richardson WH. J. Opt. Soc. Am. 1972; 62:55–59.
17. Lucy LB. Astronomical Journal. 1974; 79:745.
18. Mattson EC, Nasse MJ, Rak M, Gough KM, Hirschmugl CJ. Analytical Chemistry. 2012; 84:6173–6180. [PubMed: 22732086]
19. Choo L, Jackson M, Halliday WC, Mantsch HH. Biochimica et Biophysica Acta (BBA)-Molecular Basis of Disease. 1993; 1182:333–337.
20. Kiernan, JA. Barr's The Human Nervous System: An Anatomical View Point. 8th edn.. Lippincott Williams & Wilkins; Baltimore, MD: 2005.

21. Bhargava R, Levin IW. Analytical Chemistry. 2001; 73:5157–5167. [PubMed: 11721913]
22. Holman H-YN, Miles R, Hao Z, Wozei E, Anderson LM, Yang H. Analytical Chemistry. 2009; 81:8564–8570. [PubMed: 19775125]
23. Stavitski E, Kox MHF, Swart I, de Groot FMF, Weckhuysen BM. Angewandte Chemie, International Edition in English. 2008; 47:3543–3547.
24. Birarda G, Grenci G, Businaro L, Marmiroli B, Pacor S, Piccirilli F, Vaccari L. Vibrational Spectroscopy. 2010; 53:6–11.
25. Quaroni L, Zlateva T, Normand E. Analytical Chemistry. 2011; 83:7371–7380. [PubMed: 21854018]
26. Gardette J-L, Mailhot B. n. d. Lemaire J. Polymer Degradation and Stability. 1995; 48:457–470.
27. Ghaffar A, Scott A, Scott G. European Polymer Journal. 1976; 12:615–620.
28. Waldman WR, De Paoli MA. Polymer Degradation and Stability. 2008; 93:273–280.
29. Nasse MJ, Ratti S, Giordano M, Hirschmugl CJ. Applied Spectroscopy. 2009; 63:1181–1186. [PubMed: 19843370]
30. Tobin M, Puskar L, Barber R, Harvey E, Heraud P, Wood B, Bambery K, Dillon C, Munro K. Vibrational Spectroscopy. 2010; 53:34–38.
31. Kox MHF, Domke KF, Day JPR, Rago G, Stavitski E, Bonn M, Weckhuysen BM. Angewandte Chemie, International Edition in English. 2009; 48:8990–8994.

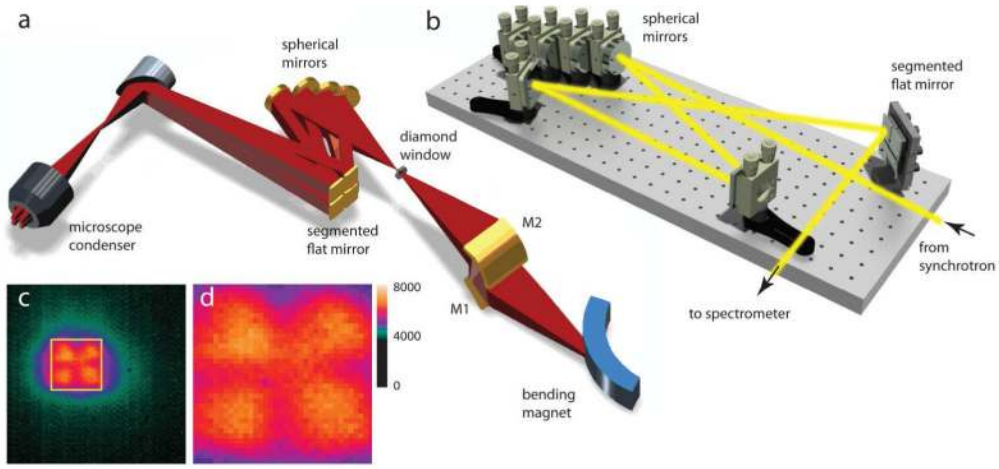

Figure 1.

(a) Schematic of the multibeam synchrotron IR imaging beamline. The bending magnet radiation (85×40 mrad) is extracted and the source is re-imaged by means of the elliptical M2 mirror. The diverging fan of light is split into four nearly collimated beamlets, which are subsequently recombined at the sample position. **(b)** Light path in the optical matching box. Only one beamlet is shown for clarity. Two folding mirrors provide additional control over the beam alignment. **(c)** Illuminated area of the 128×128 pixel FPA detector and **(d)** the enlarged FPA area of 36×36 pixels, equivalent to the sample area of 20×20 μm, showing nearly uniform illumination.

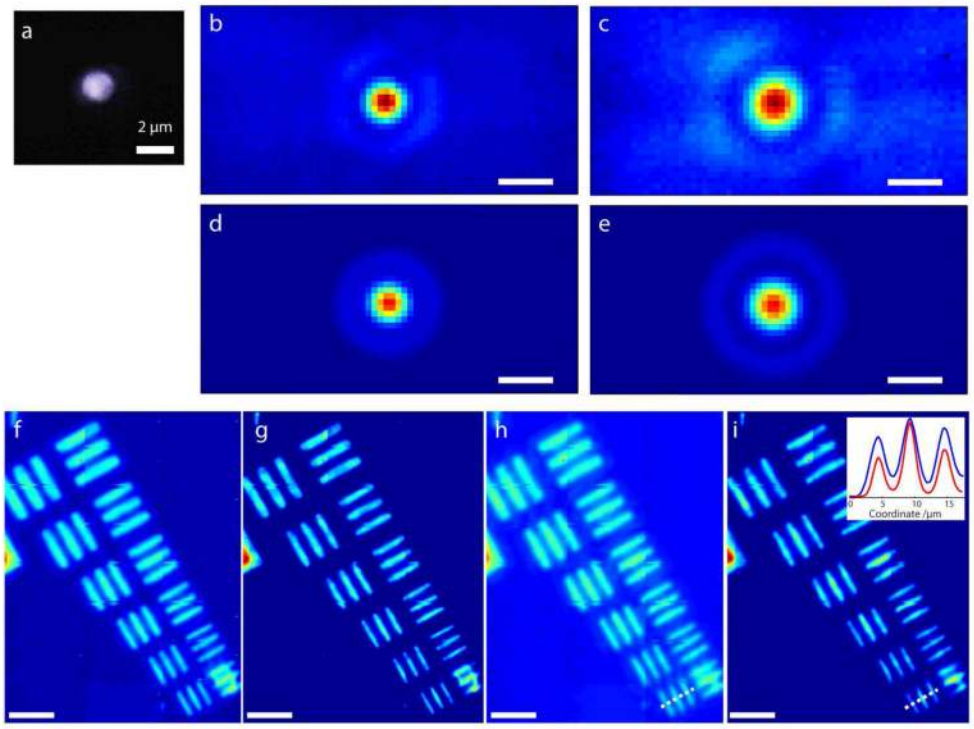

Figure 2.

Optical performance of the multibeam FTIR microscope. **(a)** Optical image of a 2 μm pinhole and **(b-c)** transmission FTIR images of the pinhole integrated from **(b)** 3200-3000 cm $^{-1}$ and **(c)** 2350-2150 cm $^{-1}$. Scale bar is 5 μm; **(d-e)** Convolution of the 2 μm pinhole with the PSF calculated for a 74× Schwarzschild reflecting objective for **(d)** 3100 cm $^{-1}$ and **(e)** 2250 cm $^{-1}$. **(f)** Transmission FTIR images of the 1951 USAF resolution test target showing Group 7 elements (line width/separation is 3.9 μm at top to 2.2 μm at bottom) intensity integrated over 3200-3000 cm $^{-1}$. Scale bar is 20 μm; **(g)** Image in **(f)** after Lucy-Richardson deconvolution using the PSF shown in **(d)**. **(h)** and **(i)** are the same as in **(f)** and **(g)** but with intensities integrated over 2350-2150 cm $^{-1}$. Inset in **(i)** shows the line profile through the smallest set of features on the pattern (2.2 μm). Blue and red lines correspond to the line profiles indicated by dashed line in **(h)** and **(i)**, respectively.

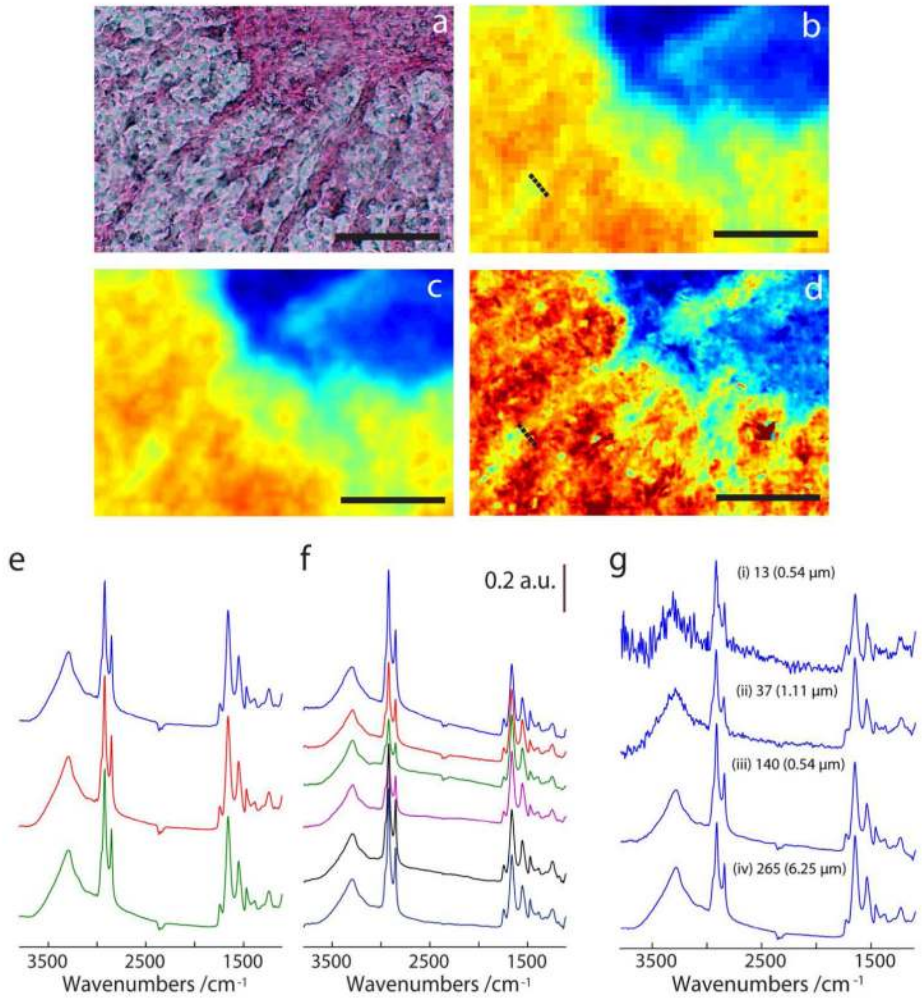

Figure 3.

FTIRI with the globar vs. multiple synchrotron beams. **(a)** Optical micrograph of the mouse spinal cord cross-section stained with eosin Y. Scale bar is 100 μm. **(b)** FTIR images showing the ratio of integrated absorbance for the C-H stretch (3000-2800 cm^{-1}) spectral regions acquired with the globar and linear array detector (6.25×6.25 μm size); **(c)** the same dataset as in **(b)** interpolated onto a mesh with 0.54 μm spacing; **(d)** same area scanned using synchrotron and FPA instrument (0.54 × 0.54 μm pixel size). Note that **(b)** - **(d)** are plotted on the same color scale; **(e)** and **(f)** Spectra from the individual pixels across the gray matter tract indicated by dashed line in **(b)** and **(d)**. **(g)** Comparison of the single-pixel spectra recorded from the spinal cord tissue sample using **(i)** globar/FPA/0.54 Nm pixel; **(ii)** globar/FPA/1.11 Nm pixel; **(iii)** synchrotron/FPA/0.54 Nm pixel, and **(iv)** globar/6.25 Nm pixel. The apparent SNR values and pixel size (in parentheses) are indicated for each spectrum.

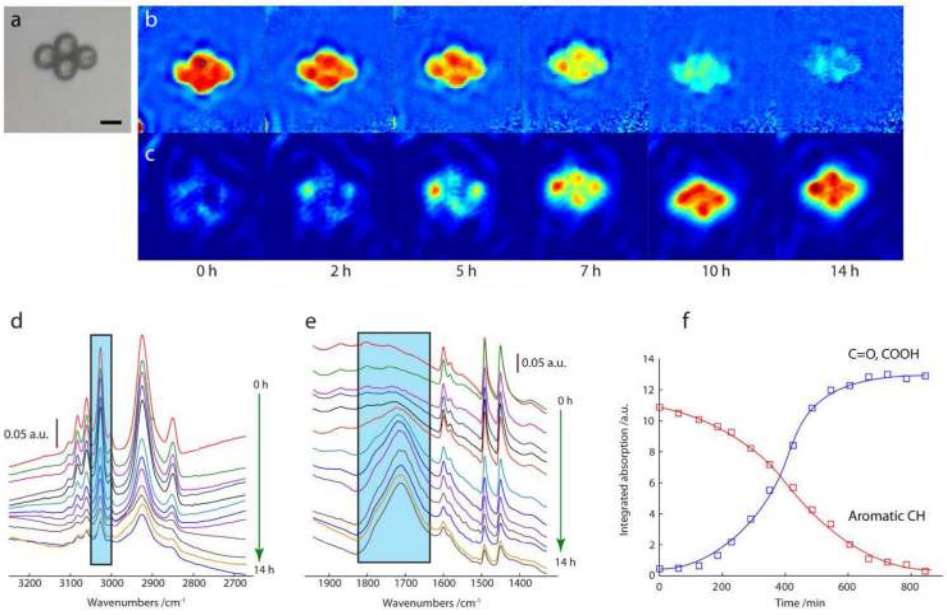

Figure 4.

time-lapsed FTIRI of the photo-oxidation of polystyrene. **(a)** Optical microphotograph of a cluster of four 5 μm polystyrene beads. FTIR images of the beads for different durations of UV exposure showing **(b)** the decrease in the C-H stretching band (3050-3000 cm^{-1}) and **(c)** the appearance of the broad carbonyl band (1620-1815 cm^{-1}). Note that the images in **(a)** and **(b)** are plotted on the same color scale. FTIR spectra of **(d)** the C-H stretch region and **(e)** the carbonyl/C-H bend regions from the UV-irradiated beads. The spectra were averaged over an area of 3×3 pixels in the center of the top bead. **(f)** Kinetics of the chemical transformations in the C-H stretching and carbonyl region, integrated over the shaded areas in **(d)** and **(e)**.